Gravitational wave asteroseismology of dark matter hadronic stars

César V. Flores[*]

Universidade Estadual da Região Tocantina do Maranhão, UEMASUL, Centro de Ciências Exatas,
Naturais e Tecnológicas, Imperatriz, CEP 65901-480 Maranhão, Brazil
and Universidade Federal do Maranhão, UFMA, Departamento de Física-CCET,
Campus Universitário do Bacanga, São Luís, CEP 65080-805 Maranhão, Brazil

C. H. Lenzi,[†] M. Dutra,[‡] and O. Lourenço[§]

Departamento de Física, Instituto Tecnológico de Aeronáutica, DCTA,
12228-900, São José dos Campos, São Paulo, Brazil

José D. V. Arbañil[‖]

Departamento de Ciencias, Universidad Privada del Norte, Avenida el Sol 461 San Juan de Lurigancho,
15434 Lima, Peru
and Facultad de Ciencias Físicas, Universidad Nacional Mayor de San Marcos,
Avenida Venezuela s/n Cercado de Lima, 15081 Lima, Peru

The influence of the dark matter mass (M_χ) and the Fermi momentum (k_F^{DM}) on the f_0-mode oscillation frequency, damping time parameter, and tidal deformability of hadronic stars are studied by employing a numerical integration of hydrostatic equilibrium, nonradial oscillation, and tidal deformability equations. The matter inside the hadronic stars follows the NL3* equation of state. We obtain that the influence of M_χ and k_F^{DM} is observed in the f_0-mode, damping tome parameter, and tidal deformability. Finally, the correlation between the tidal deformability of the GW170817 event with M_χ and k_F^{DM} are also investigated.

I. INTRODUCTION

In astrophysics, it is estimated that dark matter (DM) corresponds to approximately 27% of the matter in the Universe today. The name coined for this matter refers to the fact that it appears not to interact with light or electromagnetic field, hence the difficulty in its direct detection. However, this matter would interact gravitationally, thus leaving unequivocal observational signals of its existence [1].

The study of dark matter began in the 1930s when Fritz Zwicky observed that the velocities dispersion of galaxies within the Coma Cluster exceeded what could be accounted for by the visible matter alone [2] (review also [3]).

He suggested that an additional, unseen mass—who coined the name dark matter—must be exerting gravitational influence to accelerate these orbital motions. Subsequent investigations developed by Ford and Rubin in the 1970s [4], would show a consistent presence of unexplained high-speed orbits in every galaxy became apparent, solidifying the consensus around the existence of an exotic matter.

In the search for the exact nature of dark matter, to date, a large number of experiments have been carried out using a variety of theoretical models. Among the theoretical proposed candidates, we find weakly interacting massive particles (WIMPs) [5] and feebly interacting massive particles (FIMPS) [6,7], the neutralino [8–10], axions [11], among others; however, no concrete conclusion has been reached about the nature of dark matter. Within this set of possibilities, in particular, WIMPs are those more promising; review, for example, [12,13].

Motivated by the detections of gravitational waves caused by the merger of a binary system recorded by the LIGO-Virgo Collaboration (LVC) [14–25], in recent years, numerous investigations have explored the integration of dark matter into hadronic matter [10,26–40], as well as the effects of dark matter in relation to quarks and hybrid stars [41,42] and on some properties of neutron stars, namely, how this type of exotic matter would influence

[*]cesar.vasquez@uemasul.edu.br
[†]chlenzi@ita.br
[‡]marianad@ita.br
[§]odilon.ita@gmail.com
[‖]jose.arbanil@upn.pe

some parameters macroscopic observations such as in the equilibrium configuration [26–32], radial stability [24,25], tidal deformability [10,27,31,33–39], and f_0-mode frequency of oscillation into the Cowling approximation [40].

In the present work, we study the effect of dark matter on the stellar structure configuration, f_0-mode frequency of oscillation from complete general relativity, and tidal deformability. For the fluid inside the compact stars, we employ the relativistic mean field model with the NL3* parametrization [43]. The contribution of dark matter is included through a kinetic term as done in [33,36], where we vary the Fermi momentum by taking different values of the neutralino mass, as detailed throughout the article. Once the equation of state (EOS) is defined, the mass, radius, tidal deformability, oscillation frequency, and damping time are analyzed for both hadronic stars and for hadronic stars in a binary system. These results are contrasted with observational data reported by LVC in the articles aforementioned. In addition, the f_0-mode derived from the complete general relativity is compared with the ones derived from the nonradial oscillation equations through the Cowling approximation.

The next sections are distributed as follows. In Sec. II the structure of the hadronic model with dark matter content is described and the main equations of state of the system are obtained. In Sec. III the equilibrium equation, nonradial oscillation equation, and tidal deformability equation are presented. In Sec. IV we discuss the results and in Sec. V we conclude the paper. Finally, throughout the text, we adopt the metric signature $(-, +, +, +)$ and we employ in geometrized units $c = 1 = G$.

II. HADRONIC MODEL WITH DARK MATTER CONTENT

The impact of dark matter on the properties related to nonradial oscillations in neutron stars is performed here by considering the system, composed of hadronic matter admixed with DM, described by the following Lagrangian density:

$$\mathcal{L} = \mathcal{L}_{\text{HAD}} + \mathcal{L}_{\text{DM}}, \tag{1}$$

in which

$$\begin{aligned}
\mathcal{L}_{\text{HAD}} = &\ \bar{\psi}(i\gamma^\mu\partial_\mu - M_{\text{nuc}})\psi + g_\sigma\sigma\bar{\psi}\psi - g_\omega\bar{\psi}\gamma^\mu\omega_\mu\psi \\
&- \frac{g_\rho}{2}\bar{\psi}\gamma^\mu\vec{b}_\mu\vec{\tau}\psi + \frac{1}{2}(\partial^\mu\sigma\partial_\mu\sigma - m_\sigma^2\sigma^2) - \frac{A}{3}\sigma^3 \\
&- \frac{B}{4}\sigma^4 - \frac{1}{4}F^{\mu\nu}F_{\mu\nu} + \frac{1}{2}m_\omega^2\omega_\mu\omega^\mu - \frac{1}{4}\vec{B}^{\mu\nu}\vec{B}_{\mu\nu} \\
&+ \frac{1}{2}m_\rho^2\vec{b}_\mu\vec{b}^\mu, \tag{2}
\end{aligned}$$

with nucleon and mesons fields denoted by ψ, σ, ω^μ, and $\vec{b}_\mu$, respectively (masses given by M_{nuc}, m_σ, m_ω, and m_ρ).

The tensors $F^{\mu\nu}$ and $\vec{B}^{\mu\nu}$ are defined as $F_{\mu\nu} = \partial_\mu\omega_\nu - \partial_\nu\omega_\mu$ and $\vec{B}_{\mu\nu} = \partial_\mu\vec{b}_\nu - \partial_\nu\vec{b}_\mu$. More details of this kind of relativistic mean-field (RMF) model applied to symmetric and asymmetric nuclear matter can be found, for instance, in Refs. [44,45]. The free parameters of the model are the couplings g_σ, g_ω, g_ρ, A, B, and the particular set used here for these constants is the one given by the NL3* model [43]. Such parametrization was chosen due to its capability of reproducing ground state binding energies, charge radii, and giant monopole resonances of a set of spherical nuclei, namely, ^{16}O, ^{34}Si, ^{40}Ca, ^{48}Ca, ^{52}Ca, ^{54}Ca, ^{48}Ni, ^{56}Ni, ^{78}Ni, ^{90}Zr, ^{100}Sn, ^{132}Sn, and ^{208}Pb, as well as macroscopic properties of neutron stars. The complete study performed with more than 400 other parametrizations of the RMF model is found in Ref. [46]. The dark sector of the model is given by [10,26,27,30–36,40,47,48]

$$\begin{aligned}
\mathcal{L}_{\text{DM}} = &\ \bar{\chi}(i\gamma^\mu\partial_\mu - M_\chi)\chi + \xi h\bar{\chi}\chi + \frac{1}{2}(\partial^\mu h\partial_\mu h - m_h^2 h^2) \\
&+ f\frac{M_{\text{nuc}}}{v}h\bar{\psi}\psi, \tag{3}
\end{aligned}$$

with the Dirac field χ representing the dark fermion of mass M_χ. The scalar field h denotes the Higgs boson with mass $m_h = 125$ GeV, and the strength of the Higgs-nucleon interaction is controlled by fM_{nuc}/v, with $v = 246$ GeV being the Higgs vacuum expectation value, and $f = 0.3$ [49,50]. The constant ξ regulates the Higgs-dark particle coupling.

The field equations of the system are calculated by using the mean-field approximation [44,45], namely,

$$m_\sigma^2\sigma = g_\sigma\rho_s - A\sigma^2 - B\sigma^3, \tag{4}$$

$$m_\omega^2\omega_0 = g_\omega\rho, \tag{5}$$

$$m_\rho^2 b_{0(3)} = \frac{g_\rho}{2}\rho_3, \tag{6}$$

$$[\gamma^\mu(i\partial_\mu - g_\omega\omega_0 - g_\rho b_{0(3)}\tau_3/2) - M^*]\psi = 0, \tag{7}$$

$$m_h^2 h = \xi\rho_s^{\text{DM}} + f\frac{M_{\text{nuc}}}{v}\rho_s, \tag{8}$$

$$(\gamma^\mu i\partial_\mu - M_\chi^*)\chi = 0, \tag{9}$$

with $\tau_3 = 1$ for protons and -1 for neutrons, and effective dark particle and nucleon masses written as

$$M_\chi^* = M_\chi - \xi h, \tag{10}$$

and

$$M^* = M_{\text{nuc}} - g_\sigma\sigma - f\frac{M_{\text{nuc}}}{v}h, \tag{11}$$

respectively. The densities related to hadronic and dark sectors are

$$\rho_s = \rho_{sp} + \rho_{sn}, \tag{12}$$

$$\rho = \rho_p + \rho_n, \tag{13}$$

$$\rho_3 = \langle \bar{\psi} \gamma^0 \tau_3 \psi \rangle = \rho_p - \rho_n = (2y_p - 1)\rho, \tag{14}$$

$$\rho_{s_{p,n}} = \langle \bar{\psi}_{p,n} \psi_{p,n} \rangle = \frac{M^*}{\pi^2} \int_0^{k_{Fp,n}} \frac{k^2 dk}{(k^2 + M^{*2})^{1/2}}, \tag{15}$$

$$\rho_s^{\text{DM}} = \langle \bar{\chi} \chi \rangle = \frac{M_\chi^*}{\pi^2} \int_0^{k_F^{\text{DM}}} \frac{k^2 dk}{(k^2 + M_\chi^{*2})^{1/2}}. \tag{16}$$

The proton fraction is $y_p = \rho_p/\rho$, and the vector densities are related to the respective Fermi momenta through $\rho_{p,n} = 2k_{Fp,n}^3/(3\pi^2)$, and $\rho_\chi = 2k_F^{\text{DM3}}/(3\pi^2)$. In our study, we keep this last quantity as a free parameter, as well as the dark fermion mass, for which the values are taken from the range $50 \text{ GeV} \leq M_\chi \leq 500 \text{ GeV}$. Such interval for M_χ, along with $\xi = 0.01$, ensures that the spin-independent scattering cross-section is compatible with data provided by PandaX-II [51], LUX [52], and DarkSide [53] Collaborations.

The energy density and pressure of the system is calculated from the energy-momentum tensor, $T^{\mu\nu}$, obtained through Eq. (1). Such expressions are given, respectively, by

$$\varepsilon(\sigma, \omega_0, b_{0(3)}, \rho, y_p, h, \rho_\chi)$$
$$= \frac{m_\sigma^2 \sigma^2}{2} + \frac{A\sigma^3}{3} + \frac{B\sigma^4}{4} - \frac{m_\omega^2 \omega_0^2}{2} - \frac{m_\rho^2 b_{0(3)}^2}{2} + g_\omega \omega_0 \rho$$
$$+ \frac{g_\rho}{2} b_{0(3)} \rho_3 + \frac{m_h^2 h^2}{2} + \varepsilon_{\text{kin}}^p + \varepsilon_{\text{kin}}^n + \varepsilon_{\text{kin}}^{\text{DM}}, \tag{17}$$

and

$$P(\sigma, \omega_0, b_{0(3)}, \rho, y_p, h, \rho_\chi)$$
$$= -\frac{m_\sigma^2 \sigma^2}{2} - \frac{A\sigma^3}{3} - \frac{B\sigma^4}{4}$$
$$+ \frac{m_\omega^2 \omega_0^2}{2} + \frac{m_\rho^2 b_{0(3)}^2}{2} - \frac{m_h^2 h^2}{2} + P_{\text{kin}}^p + P_{\text{kin}}^n + P_{\text{kin}}^{\text{DM}}, \tag{18}$$

with the kinetic terms written as

$$\varepsilon_{\text{kin}}^{\text{DM}} = \frac{1}{\pi^2} \int_0^{k_F^{\text{DM}}} k^2 (k^2 + M_\chi^{*2})^{1/2} dk, \tag{19}$$

$$P_{\text{kin}}^{\text{DM}} = \frac{1}{3\pi^2} \int_0^{k_F^{\text{DM}}} \frac{k^4 dk}{(k^2 + M_\chi^{*2})^{1/2}}, \tag{20}$$

$$\epsilon_{\text{kin}}^{p,n} = \frac{1}{\pi^2} \int_0^{k_{Fp,n}} k^2 (k^2 + M^{*2})^{1/2} dk, \tag{21}$$

$$P_{\text{kin}}^{p,n} = \frac{1}{3\pi^2} \int_0^{k_{Fn,p}} \frac{k^4 dk}{(k^2 + M^{*2})^{1/2}}. \tag{22}$$

In these expressions, σ, ω_0, $b_{0(3)}$, and h are the mean-field values of the respective mesonic fields of the model.

We also include electrons and muons in the system in order to correctly describe the core of neutron stars. Therefore, energy density and pressure become

$$\epsilon_{\text{core}} = \varepsilon(\sigma, \omega_0, b_{0(3)}, \rho, y_p, h, \rho_\chi) + \frac{\mu_e^4}{4\pi^2}$$
$$+ \frac{1}{\pi^2} \int_0^{\sqrt{\mu_\mu^2 - m_\mu^2}} dk k^2 (k^2 + m_\mu^2)^{1/2}, \tag{23}$$

and

$$p_{\text{core}} = P(\sigma, \omega_0, b_{0(3)}, \rho, y_p, h, \rho_\chi) + \frac{\mu_e^4}{12\pi^2}$$
$$+ \frac{1}{3\pi^2} \int_0^{\sqrt{\mu_\mu^2 - m_\mu^2}} \frac{dk k^4}{(k^2 + m_\mu^2)^{1/2}}. \tag{24}$$

The last terms of the above equations represent the thermodynamical quantities of massless electrons, and muons with mass $m_\mu = 105.7$ MeV. The chemical potentials of these leptons, denoted by μ_e and μ_μ, are related to their respective densities through $\rho_e = \mu_e^3/(3\pi^2)$, and $\rho_\mu = [(\mu_\mu^2 - m_\mu^2)^{3/2}]/(3\pi^2)$. For a beta-equilibrated system submitted to charge neutrality, the following conditions apply, namely, $\rho_p - \rho_e = \rho_\mu$ and $\mu_n - \mu_p = \mu_e = \mu_\mu$. Finally, we consider two different regions for the description of the neutron star crust; the outer (OC) and the inner crust (IC). For the former, we use the equations proposed by Baym, Pethick, and Sutherland (BPS) [54] in a density region of $6.3 \times 10^{-12} \text{ fm}^{-3} \leq \rho \leq 2.5 \times 10^{-4} \text{ fm}^{-3}$. For the inner crust, we use a polytropic relation between energy density and pressure, namely, $p_{\text{IC}}(\epsilon_{\text{IC}}) = A + B\epsilon_{\text{IC}}^{4/3}$. We match this form to the BPS and the core equations. The latter is connected at the core-crust transition pressure and energy density, calculated through the thermodynamical method [55–57]. The total energy density and total pressure of the stellar matter are then given by

$$\epsilon = \epsilon_{\text{core}} + \epsilon_{\text{OC}} + \epsilon_{\text{IC}} \tag{25}$$

and

$$p = p_{\text{core}} + p_{\text{OC}} + p_{\text{IC}}, \tag{26}$$

respectively.

It is worth emphasizing that the equation used to determine the transition density is based on derivatives with respect to density and proton fraction, see Eq. (21) of Ref. [55] for instance. In our model, the major effect of including dark matter is due to the kinetic terms in energy density and pressure, i.e., the coupling strength is very weak and dark matter particles are essentially free particles (for a detailed discussion on this regard, we address the reader to Ref. [30]). Because of that, since such terms are taken as constants (we are fixing M_χ and k_F^{DM}), the aforementioned derivatives are not affected by dark matter. Therefore, the calculation of the transition density is not impacted either.

III. GENERAL RELATIVISTIC FORMALISM

A. The stellar equilibrium equations

The static equilibrium configurations of a compact star composed of a perfect fluid are obtained through the Tolman-Oppenheimer-Volkoff (TOV) equations,

$$\frac{dp}{dr} = -\frac{\epsilon m}{r^2}\left(1 + \frac{p}{\epsilon}\right)\left(\frac{1 + \frac{4\pi p r^3}{m}}{1 - \frac{2m}{r}}\right), \qquad (27)$$

$$\frac{d\nu}{dr} = -\frac{2}{\epsilon}\frac{dp}{dr}\left(1 + \frac{p}{\epsilon}\right)^{-1}, \qquad (28)$$

$$\frac{dm}{dr} = 4\pi r^2 \epsilon. \qquad (29)$$

The variables $m(r)$ and $\nu(r)$ are respectively the gravitational mass inside the radius r and a metric potential. The pressure p and the mass-energy density ϵ are connected by the equations of state. To integrate the system of Eqs. (27)–(29) from the center ($r = 0$) to the star's surface ($r = R$), some conditions are required. At the center of the star ($r = 0$), we have

$$\epsilon(0) = \epsilon_c, \qquad p(0) = p_c, \quad \text{and} \quad m(0) = 0. \qquad (30)$$

The surface of the star is found when $p(R) = 0$. At this point

$$\nu(R) = \ln\left(1 - \frac{2M}{R}\right), \qquad (31)$$

with M representing the total stellar mass.

B. The nonradial oscillation equations

To investigate the nonradial oscillation, both spacetime and fluid variables are perturbed. The perturbations are replaced in the Einstein field equation, in the energy-momentum tensor, and in the baryon number conservation maintaining only the first-order variables.

Following Refs. [58,59], we adopt the perturbed line element of the form,

$$\begin{aligned} ds^2 = &-e^\nu(1 + r^\ell H_0 Y_m^\ell e^{i\omega t})dt^2 - 2i\omega r^{\ell+1} H_1 Y_m^\ell e^{i\omega t}dtdr \\ &+ e^\lambda(1 - r^\ell H_0 Y_m^\ell e^{i\omega t})dr^2 \\ &+ r^2(1 - r^\ell K Y_m^\ell e^{i\omega t})(d\theta^2 + \sin^2\theta d\phi^2), \end{aligned} \qquad (32)$$

with $H_0 = H_0(r)$, $H_1 = H_1(r)$, and $K = K(r)$ being functions of the radial coordinate r only, ω depicting the eigenfrequency of oscillation, and $Y_m^\ell = Y_m^\ell(\theta, \phi)$ representing the even-parity spherical harmonic functions. Since the small perturbations are set by the Lagrangian fluid displacement ξ^β, we consider:

$$\xi^r = r^{\ell-1} e^{-\lambda/2} W Y_m^\ell e^{i\omega t}, \qquad (33)$$

$$\xi^\theta = -r^{\ell-2} V \partial_\theta Y_m^\ell e^{i\omega t}, \qquad (34)$$

$$\xi^\phi = -r^\ell (r\sin\theta)^{-2} V \partial_\phi Y_m^\ell e^{i\omega t}, \qquad (35)$$

where $\xi^0 = 0$.

With this, nonradial oscillations are described by the following set of first-order linear differential equations [59]:

$$\begin{aligned} H_1' = &-r^{-1}\left[\ell + 1 + \frac{2Me^\lambda}{r} + 4\pi r^2 e^\lambda(p - \epsilon)\right]H_1 \\ &+ e^\lambda r^{-1}[H_0 + K - 16\pi(\epsilon + p)V], \end{aligned} \qquad (36)$$

$$\begin{aligned} K' = &r^{-1}H_0 + \frac{\ell(\ell+1)}{2r}H_1 - \left[\frac{(\ell+1)}{r} - \frac{\nu'}{2}\right]K \\ &- 8\pi(\epsilon + p)e^{\lambda/2}r^{-1}W, \end{aligned} \qquad (37)$$

$$\begin{aligned} W' = &-(\ell+1)r^{-1}W + re^{\lambda/2}\left[e^{-\nu/2}\gamma^{-1}p^{-1}X \right. \\ &\left. - \ell(\ell+1)r^{-2}V + \frac{1}{2}H_0 + K\right], \end{aligned} \qquad (38)$$

$$\begin{aligned} X' = &-\ell r^{-1}X + \frac{(\epsilon + p)e^{\nu/2}}{2}\left[\left(\frac{1}{r} + \frac{\nu'}{2}\right)H_0 \right. \\ &+ \left(r\omega^2 e^{-\nu} + \frac{\ell(\ell+1)}{2r}\right)H_1 + \left(\frac{3}{2}\nu' - \frac{1}{r}\right)K \\ &- \ell(\ell+1)r^{-2}\nu'V - 2r^{-1}\left(4\pi(\epsilon + p)e^{\lambda/2}\right. \\ &\left.\left. + \omega^2 e^{\lambda/2-\nu} - \frac{r^2}{2}(e^{-\lambda/2}r^{-2}\nu')'\right)W\right], \end{aligned} \qquad (39)$$

where the prime stands a derivative with respect to r and γ depicts the adiabatic index. The function X is given by

$$X = \omega^2(\epsilon + p)e^{-\nu/2}V - \frac{p'}{r}e^{(\nu-\lambda)/2}W$$
$$+ \frac{1}{2}(\epsilon + p)e^{\nu/2}H_0, \tag{40}$$

with H_0 fulfilling the algebraic relation

$$a_1 H_0 = a_2 X - a_3 H_1 + a_4 K, \tag{41}$$

where

$$a_1 = 3M + \frac{1}{2}(l+2)(l-1)r + 4\pi r^3 p, \tag{42}$$

$$a_2 = 8\pi r^3 e^{-\nu/2}, \tag{43}$$

$$a_3 = \frac{1}{2}l(l+1)(M + 4\pi r^3 p) - \omega^2 r^3 e^{-(\lambda+\nu)}, \tag{44}$$

$$a_4 = \frac{1}{2}(l+2)(l-1)r - \omega^2 r^3 e^{-\nu}$$
$$- r^{-1}e^{\lambda}(M + 4\pi r^3 p)(3M - r + 4\pi r^3 p). \tag{45}$$

Outside the stellar structure configuration, the perturbation functions that describe the motion of the fluid W and V vanish, and the system of differential equations reduces to the Zerilli equation,

$$\frac{d^2 Z}{dr^{*2}} = [V_Z(r^*) - \omega^2]Z, \tag{46}$$

where $Z(r^*)$ and $dZ(r^*)/dr^*$ are related to the functions $H_0(r)$ and $K(r)$ through the transformations given in Refs. [58,59]. $Z(r^*)$ depends on the "tortoise" coordinate which is given by

$$r^* = r + 2M \ln\left(\frac{r}{2M} - 1\right), \tag{47}$$

and the effective potential $V_Z(r^*)$ yields

$$V_Z(r^*) = \frac{(1 - 2M/r)}{r^3(nr + 3M)^2}[2n^2(n+1)r^3 + 6n^2 Mr^2$$
$$+ 18nM^2 r + 18M^3], \tag{48}$$

with $n = (l-1)(l+2)/2$.

For given values of l and ω, the set of Eqs. (36)–(39) has four linearly independent solutions. The physical solution obtained must verify boundary conditions: (a) The perturbation functions have to be regular throughout the entire star; thus implying that in $r = 0$ must also be finite, since at this point nonradial oscillation equations are singular. To insert such condition, the solution near $r = 0$ must be expanded using a power series (for more detail about the process, see Ref. [58]); (b) Since the Lagrangian perturbation

of pressure vanishes at the star's surface $r = R$. This boundary condition is equivalent to $X(R) = 0$. For a set of values of l and ω, there is a solution that fulfills the above boundary conditions inside the star.

In general, in the exterior of the star, the perturbed line element depicts a mixture of outgoing and ingoing gravitational waves. Since we focus on the purely outgoing gravitational radiation at $r = \infty$, the Zerilli equation is used. The eigenfrequency of oscillation that satisfies this requirement represents the quasinormal modes of the stellar model. The process to solve the above equations is detailed in [58,59].

Different oscillation modes can be investigated using the aforementioned equations. The purely gravitational modes (w-modes) do not induce fluid motion and are highly damped. The fluid pulsation modes (f_0, g, and p-modes) are usually grouped according to the origin of the restoring force that prevails in bringing the perturbed element of fluid back to the equilibrium position; e.g., the buoyancy in the case of g-modes or a gradient of pressure for p-modes. It is widely known that the frequencies of the g-modes are lower than those of p-modes, and these two sets are separated by the frequency of the f_0-mode. The f_0-mode frequency is proportional to the square root of the mean density of the star and tends to be independent of the details of the stellar structure. In this work, we analyze only the f_0-mode because it is expected to be the most excited in astrophysical events and, therefore, the one that contributes the most to the emission of gravitational waves coming from a star.

C. The tidal deformability equations

The analysis of tidal deformability is commonly investigated in binary compact object systems. The gravitational effects caused by one star can bring out the deformation of its partner. This deformation was investigated by Damour and Nagar, Binnington and Poisson [60,61]. They found that the tidal deformation of a neutron star is determined by the gravitoelectric K_2^{el} and gravitomagnetic K_2^{mag} Love numbers, which are respectively connected with the mass quadrupole and with the current quadrupole induced by the companion star. Additional research carried out by Flanagan and Hindeler found that a single detection should be sufficient to impose upper limits on K_2^{el} at 90% confidence level [62]. Since then, intensive research has been carried out on the calculation of the Love numbers of neutron stars [63–67].

In a binary stellar system, the induced quadrupole moment Q_{ij} in one neutron star because of the external tidal field $\mathcal{E}_{ij}$ induced by a partner compact object can be expressed as [67]

$$Q_{ij} = -\lambda \mathcal{E}_{ij}, \tag{49}$$

where λ is the tidal deformability parameter, which can be written in terms of the quadrupole ($l = 2$) tidal Love number k_2 as

$$\lambda = \frac{2}{3} k_2 R^5. \tag{50}$$

To determine k_2 we need to solve the first-order differential equation,

$$r\frac{dy}{dr} + y^2 + yF(r) + r^2 Q(r) = 0, \tag{51}$$

with the functions $F(r)$ and $Q(r)$ given by

$$F(r) = [1 - 4\pi r^2(\varepsilon - p)]/E \tag{52}$$

$$Q(r) = 4\pi \left[5\varepsilon + 9p + (\varepsilon + p)\left(\frac{\partial p}{\partial \varepsilon}\right) - \frac{6}{4\pi r^2}\right] \Big/ E$$
$$- 4\left[\frac{m + 4\pi r^3 p}{r^2 E}\right]^2, \tag{53}$$

with $E = 1 - 2m/r$. Therefore the Love number k_2 is computed to be

$$k_2 = \frac{8C^5}{5}(1 - 2C)^2[2 + C(y_R - 1) - y_R]$$
$$\times \{2C[6 - 3y_R + 3C(5y_R - 8)]$$
$$+ 4C^3[13 - 11y_R + C(3y_R - 2) + 2C^2(1 + y_R)]$$
$$+ 3(1 - 2C^2)[2 - y_R + 2C(y_R - 1)]\ln(1 - 2C)\}^{-1}, \tag{54}$$

where the function $y_R = y(r = R)$ and $C = M/R$ is the compactness parameter. Equation (51) has to be solved coupled with the TOV equations.

The dimensionless tidal deformability Λ (i.e., the dimensionless version of λ) is connected with the Love number through the relation

$$\Lambda = \frac{2k_2}{3C^5}. \tag{55}$$

IV. RESULTS

A. General remarks

In this work, the full general relativistic equations for the oscillations of neutron stars (perturbations on fluid and spacetime variables are coupled) are considered. In this case, the oscillations (for $l = 2$, i.e., quadrupole oscillations) are coupled with gravitational radiation. For a further double-check of our results, we also consider the well-known Cowling approximation, where it is considered that the fluid perturbations are weakly coupled with the spacetime vibrations. In this case, we have only a set of differential equations for the fluid variables.

For the results obtained by using the Cowling approximation, we employ a code that implements the shooting method. In this procedure, there exist boundary conditions to be considered in the center and on the surface of the star. In the first stage, in the center of the star, we consider the initial values of the functions W and V (which satisfy regularity conditions), and we also introduce a trial value for the f_0-mode frequency, which is typically around 2.5 kHz (Of course, this shoot is suitable for a standard neutron star). After setting the initial values for the fluid variables and the initial value for the frequency, we proceed with the numerical integration which starts in the center and ends on the surface of the star; this numerical integration is developed using the Runge Kutta method. After finishing the integration process, we arrive at the surface of the star, and at this point, we use the Newton-Raphson method to see if the estimated frequency value (the value of the eigenfunction) satisfies the boundary condition. If we do not find a good precision, the test value for the frequency is corrected and the integration process is initialized again, until we have the desired precision for the oscillation mode. This Cowling frequency will be used to obtain good convergence in the numerical treatment of the full general relativistic equations, and at the same time that frequency works as a good double-check for our results. Also, this numerical code allows us to obtain the f_0-mode reported in the literature, e.g., it reproduces the results of Ref. [68].

In a more rigorous treatment of neutron star seismology, we have to consider the coupling between the fluid movement and the metric perturbations. In this case, the numerical procedure is a very elaborate and long process of shooting method. The first step is to use as our best test value for the gravitational wave frequency the one obtained in the framework of the Cowling approximation, i.e., ω_{Cow}. With such proof value, we begin the integration inside the star, from the center towards the star's surface. At first, it is selected three linearly independent solutions compatible with the regularity conditions in the center of the star, and then we begin with the numerical integration from $r = 0$ to the point $R/2$ inside the star. After that, a second integration is realized, where we select two linearly independent solutions compatible with the boundary condition on the star's surface, this process is made from the surface R to the point $R/2$. To complete the procedure inside the star, the five solutions are combined to obtain compatibility with the boundary conditions at the center and on the surface of the star. Thereafter, we continue with the integration outside the star. The boundary values for the Zerilli function and its derivative at the surface of the star can always be obtained from the values of $H_0(R)$ and $K(R)$ obtained from the integration inside the compact star. Then, $Z(r^*)$ can be determined outside the star by integrating the Zerilli equation. At an asymptotically large radius (which represents the infinity), the two linearly independent solutions of the Zerilli equation may be expressed as power series

$$Z_-(r^*) = e^{-i\omega r^*} \sum_{j=0}^{\infty} \beta_j r^{-j} \qquad (56)$$

and

$$Z_+(r^*) = e^{i\omega r^*} \sum_{j=0}^{\infty} \bar{\beta}_j, \qquad (57)$$

where Z_- depicts the radiated waves and Z_+ the ingoing waves. The general asymptotic solution is given by the linear combination

$$Z(r^*) = A(\omega)Z_-(r^*) + B(\omega)Z_+(r^*), \qquad (58)$$

with $A(\omega)$ and $B(\omega)$ being complex numbers. The integration of the Zerilli differential equation from the surface of the star to the infinity ($r_\infty \approx 55\omega^{-1}$) allows finding Z and dZ/dr. Then, by using $Z(r^*)$ at $r^* = r^*_\infty$, we can obtain $B(\omega) = 0$ against to $Z(r^*_\infty)$ and $dZ/dr(r^*_\infty)$ for each value of ω. The boundary condition at infinity requires that we only have outgoing gravitational radiation, i.e., to find the frequencies of quasinormal modes we must obtain the roots of $B(\omega) = 0$. This is achieved by determining $B(\omega)$ for three different close trial values of the eigenfrequency ω. Then, we fit a quadratic polynomial $B(\omega) = \gamma_0 + \gamma_1 \omega + \gamma_2 \omega^2$ to the computed values of ω to obtain an approximate root of $B(\omega) = 0$. Finally, we iterate this procedure using the real part of the approximate root as an input for the next integration of the oscillation equations. This interaction is repeated until the real part value of the quasinormal mode changes from one step to the next by less than one part in 10^8. The imaginary part of ω is connected to the gravitational damping time of the oscillation τ. The numerical code implemented in this case allows us to reproduce the results shown in Ref. [69].

In this work, we analyze the effects of dark matter inside neutron stars. Since dark matter would interact very weakly with normal matter, its possible effects just could be felt only in a gravitational field.

For our purposes, the dark matter mass M_χ and the Fermi momentum of dark matter particles k_F^{DM} values were selected to satisfy the restrictions obtained of both stellar mass and the tidal deformability of neutron stars observed; namely, we use $M_\chi = 50$ MeV, 200 MeV, and 500 MeV and $k_F^{DM} = 0$ GeV, 0.02 GeV, 0.04 GeV, and 0.06 GeV. As a consequence, by using the NL3* EOS, we reproduce the mass, radius, f_0-mode frequency, damping time of the fundamental mode, and tidal deformability.

B. Tidal deformability, frequency of oscillations, and damping time of fundamental mode for a hadronic star

From Fig. 1, the mass, normalized in solar masses, as a function of the total radius is plotted for some values of M_χ and k_F^{DM}. The observation data belong to the NICER restrictions obtained from the pulsars PSR J0030 + 0451 [70,71] and PSR J0740 + 6620 [72,73]. There are also
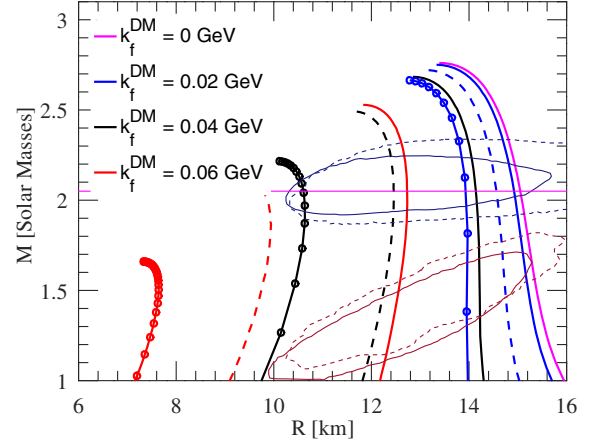

FIG. 1. Mass, normalized in Sun's masses, versus radius for some values of M_χ and k_F^{DM}. The curve in magenta represents the case without dark matter. The curves of the same color represent the results for a fixed value of k_F^{DM} and the curves of the same type depict results for a fixed value of M_χ. The solid curves correspond to $M_\chi = 50$ MeV, dashed curves correspond to $M_\chi = 200$ MeV, and solid curves with circles correspond to the case $M_\chi = 500$ MeV. Red and blue regions represent the masses and radii intervals (95%) from PSR J0030 + 0451 and PSR J0740 + 6620 measured by NICER [70–73]. The magenta horizontal line includes all observed neutron stars over 2 solar masses, which include the pulsars PSR $J1614 - 2230$, PSR J0348 + 0432, and PSR J0740 + 6620 [74–76].
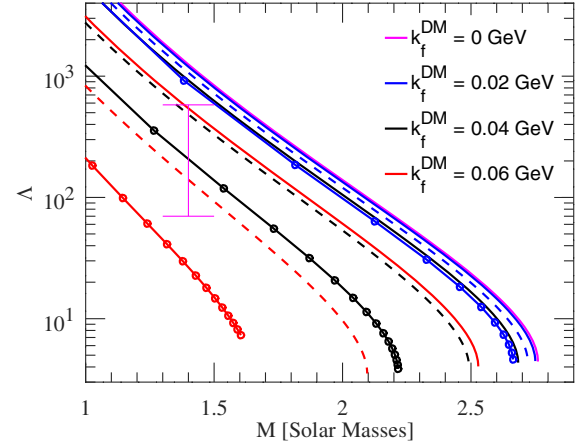

FIG. 2. Tidal deformability versus mass different values of M_χ and k_F^{DM}. The curve in magenta stands for the case without dark matter. The curves with the same type of color represent results obtained with the same value of k_F^{DM} and the curves of the same type depict the results found with the same value M_χ. The solid curves correspond to $M_\chi = 50$ MeV, dashed curves correspond to $M_\chi = 200$ MeV, and solid curves with circles correspond to the case $M_\chi = 500$ MeV. The vertical solid line depicts $\Lambda_{1.4} = 190^{+390}_{-120}$ published in Ref. [23].

shown the bands of the pulsars PSR J0740 + 6620 [74], PSR J0348 + 0432 [75], and PSR J1614 + 2230 [76]. In the figure, we observe that there is a strong dependence of the stellar mass on the parameters M_χ and k_F^{DM}. For a fixed M_χ, an increase of k_F^{DM} bring as a consequence a decrease of the maximum mass. It means that the increase in the Fermi momentum of dark matter produces a softness in the EOS, therefore there is a lower pressure, thus obtaining an equilibrium configuration with lower masses. In the same figure, we also observe that an increase in M_χ induces a decrease in the stellar mass; i.e., we have a softer EOS when that parameter is increased. From these results, we observe that the change of M_χ and k_F^{DM} allows us to find some results more precise and closer to empirical evidence of neutron stars PSR J0030 + 0451, PSR J0740 + 6620, PSR J0740 + 6620, PSR J0348 + 0432, and PSR J1614 + 2230.

The deformation of a compact star within a binary system is measured by the tidal deformability Λ. In this way, Fig. 2 shows the deformability parameter as a function of the mass. These results are compared with the case $\Lambda_{1.4} = 190^{+390}_{-120}$ reported by LVC in [23]. In all curves, we found a monotonic decay of the deformability with the increment of the mass. In addition, we observe the effects of the quantities M_χ and k_F^{DM} on the tidal deformability. For an interval of total masses, we note that lower values Λ are obtained when larger values of both M_χ and k_F^{DM} are used. Note that there are curves that are into the interval $\Lambda_{1.4}$ described by LVC in [23].

Since our objective is to determine a relationship between the mass stellar configuration, tidal deformability, and frequency of the fundamental mode we plot the f_0-mode frequency and its respective damping time as a function of the total mass on the top panel of Fig. 3 and against the tidal
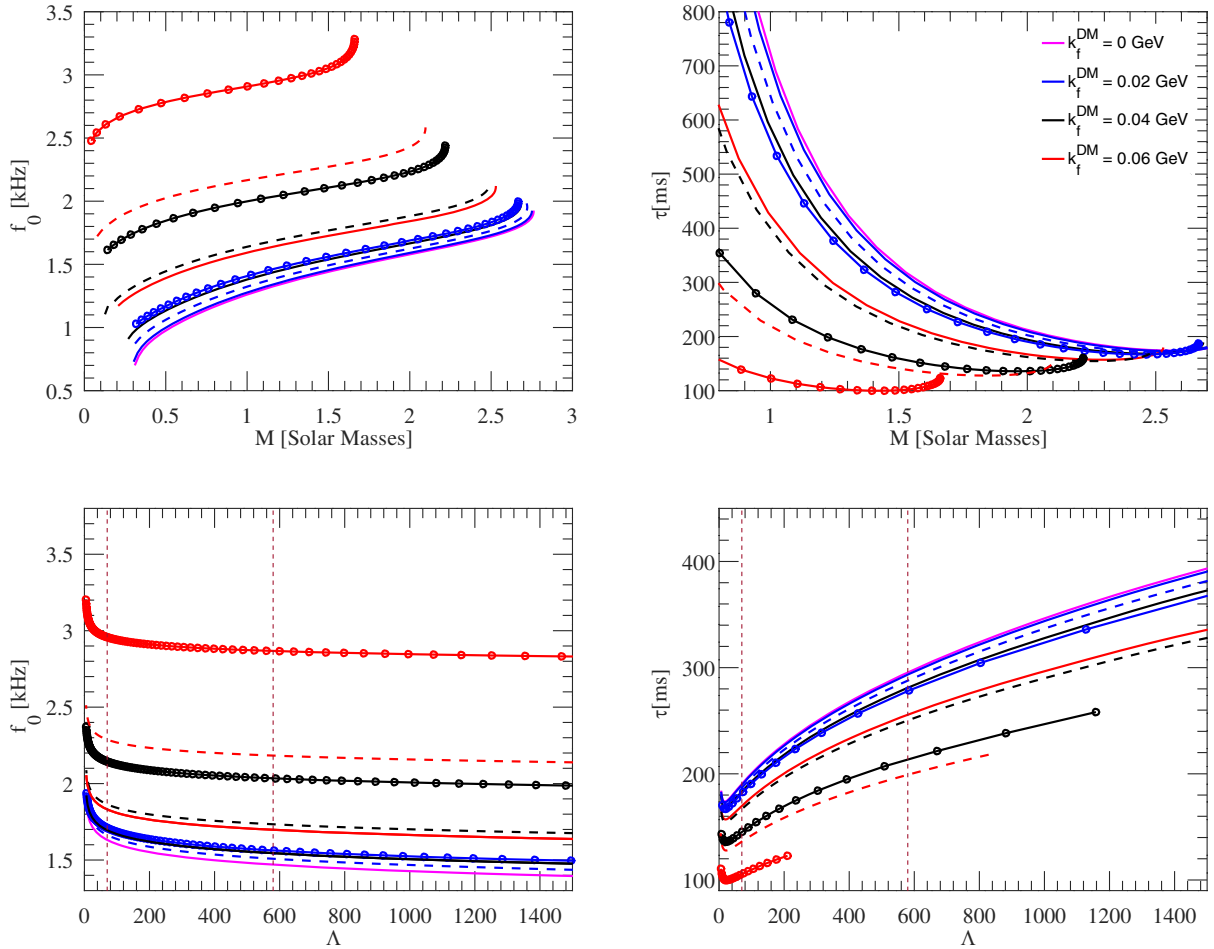

FIG. 3. Fundamental mode frequency f_0 and damping time of fundamental mode τ against the total mass $M/M_\odot$ are shown on the top panel and versus the tidal deformability Λ on the bottom panel. In all cases, different values of M_χ and k_F^{DM} are employed. The curves in magenta depict the case without dark matter. The curves of the same color represent the results for a fixed value of k_F^{DM} and the curves of the same type stand results for a fixed value of M_χ. The solid curves correspond to $M_\chi = 50$ MeV, dashed curves correspond to $M_\chi = 200$ MeV, and solid curves with circles correspond to the case $M_\chi = 500$ MeV. In the bottom panels, the dashed vertical lines represent the tidal deformability obtained from the event GW170817, i.e., $\Lambda_{1.4} = 190^{+390}_{-120}$, reported Ref. [23].

TABLE I. Maximum mass values M_{max}, and their corresponding radius R, fundamental mode frequency f_0, and damping time of the fundamental mode τ, calculated for different values of Fermi moment of dark matter k_F^{DM} and dark matter mass M_χ.

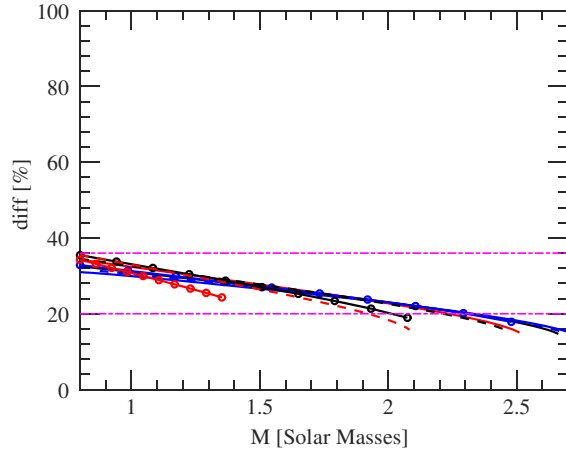| k_F^{DM} (GeV)	M_χ (MeV)	M_{max} ($M_\odot$)	R (km)	f_0 (kHz)	τ (s)
0.00	$\cdots$	2.760	13.39	1.930	1.940
0.02	50	2.750	13.33	1.920	1.920
	200	2.720	3.110	1.980	1.940
	500	2.670	12.72	2.000	1.870
0.04	50	2.680	12.85	1.990	1.890
	200	2.690	11.61	2.150	1.780
	500	2.220	10.08	3.280	1.230
0.06	50	2.520	11.83	2.120	1.780
	200	2.100	9.450	2.580	1.520
	500	1.660	7.330	3.280	1.230

FIG. 4. The relative difference between the frequency of the fundamental mode in the full linearized equations and the relativistic Cowling approximation, diff $= 100 \times (f_0 - f_0^{\text{cow}})/f_0$, versus the total mass for all M_χ and k_F^{DM} considered in Fig. 4.

deformability on the bottom panel of Fig. 3, where are employed for different values of M_χ and k_F^{DM}. The results on the bottom panels are compared with the tidal deformability derived from the event GW170817, $\Lambda_{1.4} = 190^{+390}_{-120}$, communicated in [23]. These plots have justification in the physics of the binary system because when both stars are orbiting each other, there could exist resonance and, in principle, the fundamental mode of both stars could be excited. In this way, in this figure, we see the change in M_χ and k_F^{DM} produces a systematic shifting in the curves of $f_0(M), \tau(M), f_0(\Lambda)$, and $\tau(\Lambda)$; review also Table I to see the change of the maximum total masses with their respective parameters R, f_0, and τ with M_χ and k_F^{DM} employed in Fig. 3. Moreover, in the range placed by the observation, we see that the f_0-mode frequency has a nearly linear behavior. In addition, the frequency of the f_0 mode obtained in the full-linearized equations of general relativity is compared with the relativistic Cowling approximation in Fig. 4. We found that the f_0-mode with the approximation differs by less than about 40%, in low-mass stars, and differs by less than about 20%, in high-mass stars.

The f_0-mode frequency of oscillations, damping time mode, and tidal deformability as a function of the Fermi momentum of dark matter are shown in Fig. 5 for three values of dark matter mass $M_\chi = 50$ MeV, 200 MeV, and 500 MeV. The results presented correspond to the equilibrium configuration with total mass $M = 1.4 M_\odot$. The curves $\Lambda \times k_F^{\text{DM}}$ are constrasted with the case $\Lambda_{1.4} = 190^{+390}_{-120}$ reported by LVC in Ref. [23]. From the figure, we see that equilibrium solutions with 1.4 solar masses with larger f_0-mode frequency and lower tidal deformability are found when higher values of k_F^{DM} and M_χ are considered.

C. Tidal deformability, frequency of oscillations, and damping time of fundamental mode for a binary hadronic star system

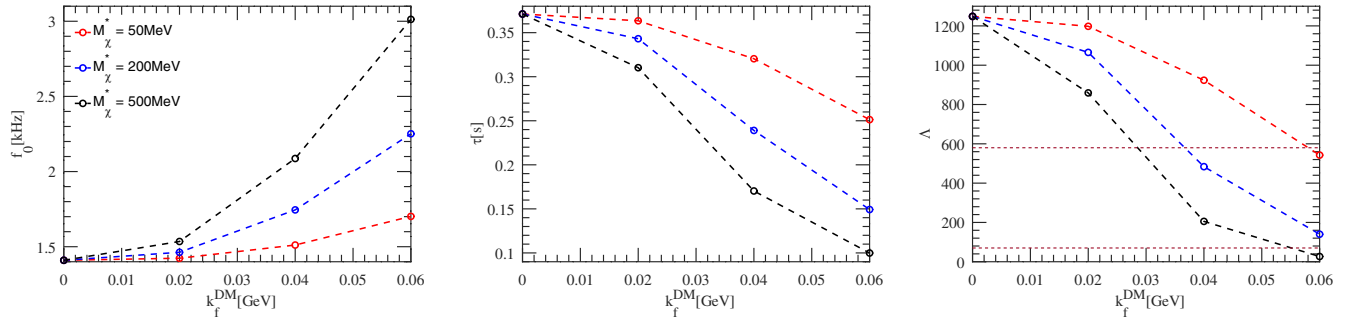In Ref. [22], by using the data reported by LVC, authors implement some constraints on the dimensionless tidal
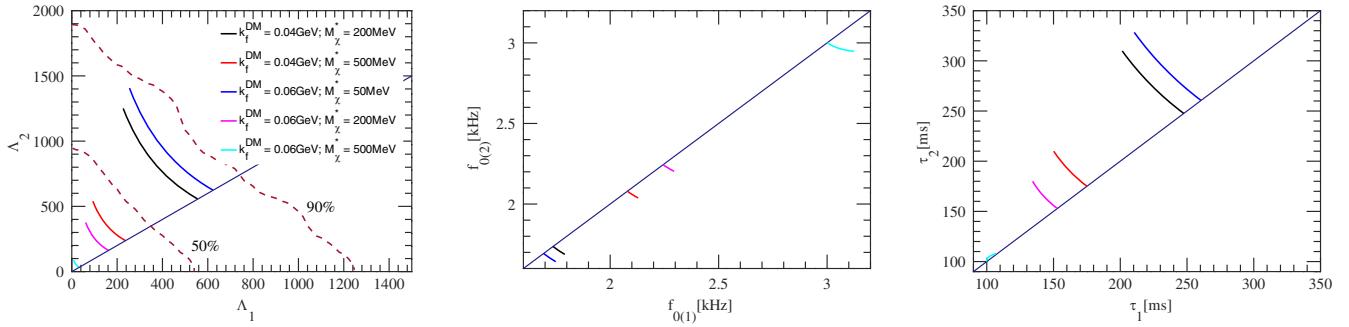

FIG. 5. The f_0-mode oscillation frequency, damping time parameter, and tidal deformability against the Fermi momentum of dark matter are shown respectively on the left, middle, and right panels. The results connected on straight dashed lines on red, blue, and black correspond to $M_\chi = 50$ MeV, 200 MeV, and 500 MeV. All values presented concern the equilibrium configurations with total masses $M = 1.4 M_\odot$. The horizontal straight line represent $\Lambda_{1.4} = 190^{+390}_{-120}$ obtained by LVC in Ref. [23].

FIG. 6.   In the Left, middle, and bottom panels are respectively plotted $\Lambda_2 \times \Lambda_1$, $f_{0(2)} \times f_{0(1)}$, and $\tau_2 \times \tau_1$ for the components of the event GW170817 for different values of $k_F^{\rm DM}$ and M_χ. The wine lines on the left panel depict the LIGO-Virgo confidence curves of 50% and 90% levels [22] and the solid diagonal appearing on the left, middle, and right panels correspond respectively to $\Lambda_1 = \Lambda_2$, $f_{0(1)} = f_{0(2)}$, and $\tau_1 = \tau_2$.

deformability of a binary system Λ_1 and Λ_2, with Λ_1 representing a star's dimensionless tidal deformability in the system and Λ_2 depicting the same parameter but of its companion. In this way, in Fig. 6, we present the relation $\Lambda_2 \times \Lambda_1$, where the numerical results are obtained by choosing a value of M_1 and finding M_2 through the chirp mass $M = 1.188 M_\odot$ [22] which is determined by

$$M = \frac{(M_1 M_2)^{3/5}}{(M_1 + M_2)^{1/5}}. \qquad (59)$$

In addition, the value of M_1 and M_2 are respectively in the interval $1.36 M_\odot \leq M_1 \leq 1.60 M_\odot$ and $1.17 M_\odot \leq M_2 \leq 1.36 M_\odot$. In the figure are also placed the credibility levels linked to the GW170817 event instituted by LVC in the low-spin prior scenario. We note that the larger values of $k_F^{\rm DM}$ and lower values of M_χ, and vice versa, allow us to obtain values within the confidence lines extracted from Ref. [22]. In Fig. 6 also appears the curves $f_0(2) \times f_0(1)$ and $\tau_2 \times \tau_1$ for the same binary system. In these two relations, for all values of $k_F^{\rm DM}$ and M_χ considered, we see the dependence of the frequency and the damping time of one star concerning its partner. In the first one, we note that $f_{0(2)}$ decays with the increment of $f_{0(1)}$ and in the second one τ_2 grows with the decline of τ_1.

V. CONCLUSIONS

In the present article, we study the effects of the dark matter mass M_χ and the Fermi momentum of dark matter particles $k_F^{\rm DM}$ in the fluid pulsation mode, damping time parameter, and tidal deformability of hadronic stars. These studies are developed by the numerical integration of the hydrostatic equilibrium, nonradial oscillation, and tidal deformability equations. The matter within the stars is considered the NL3* equation of state.

About the total mass, it is observed that it changes notoriously with M_χ and $k_F^{\rm DM}$. From an appropriate

combination of M_χ and $k_F^{\rm DM}$, we can determine that some solutions that are close to the empirical evidence of neutron stars PSR J0030 + 0451, PSR J0740 + 6620, PSR J0740 + 6620, PSR J0348 + 0432, and PSR J1614+ 2230.

Concerning the fluid pulsation mode, damping time parameter, and tidal deformability, they are considerably affected by M_χ and $k_F^{\rm DM}$. We found that the f_0-mode grows with M_χ and $k_F^{\rm DM}$ and the damping time and tidal deformability decay with these parameters. We also contrast these results with the observational reported by the LVC from the GW170817 event. In this scheme, the numerical results reported are in the range of the observational data aforementioned.

We also calculated the frequencies of the fundamental mode by using the Cowling approximation, as done in the reference [40]; where the authors showed that dark matter affects the f-mode frequency in the RMF model with and without hyperons. In our model, it was derived the same effect in the presence of dark matter in hadronic stars. We showed that for larger mass values, the Cowling method provides a good approximation compared to the solution of the complete equation; the difference between these two models is below 20% for stars with masses above $2 M_\odot$ (see Fig. 4).

The influence of M_χ and $k_F^{\rm DM}$ on the tidal deformability, f-mode frequency, and damping time parameter for a binary hadronic star system with equal chirp mass as the GW170817 event have been also studied. We found the dependence of $f_{0(1)}$-mode, τ_1, and Λ_1 of one star with $f_{0(2)}$-mode, τ_2, and Λ_2 of its partner and how these relations change with the dark matter mass and the Fermi momentum of dark matter particles.

[1] N. Aghanim, Y. Akrami, M. Ashdown, J. Aumont, C. Baccigalupi, M. Ballardini, A. J. Banday, R. B. Barreiro, N. Bartolo, S. Basak, R. Battye, K. Benabed *et al.* (Planck Collaboration), Astron. Astrophys. **641,** A6 (2020).

[2] F. Zwicky, Helv. Phys. Acta **6**, 110 (1933), https://ui.adsabs.harvard.edu/abs/1933AcHPh...6..110Z/abstract.

[3] H. Andernach and F. Zwicky, arXiv:1711.01693.

[4] V. Rubin and W. Ford, Astrophys. J. **159**, 379 (1970).

[5] C. Kouvaris and P. Tinyakov, Phys. Rev. D **83**, 083512 (2011).

[6] N. Bernal, M. Heikinheimo, T. Tenkanen, K. Tuominen, and V. Vaskonen, Int. J. Mod. Phys. A **32**, 1730023-274 (2017).

[7] L. J. Hall, K. Jedamzik, J. March-Russell, and S. M. West, J. High Energy Phys. 03 (2010) 080.

[8] D. Hooper and L.-T. Wang, Phys. Rev. D **69**, 035001 (2004).

[9] T. Han, Z. Liu, and S. Su, J. High Energy Phys. 08 (2014) 093.

[10] A. Das, T. Malik, and A. C. Nayak, Phys. Rev. D **99**, 043016 (2019).

[11] L. D. Duffy and K. van Bibber, New J. Phys. **11**, 105008 (2009).

[12] G. Bertone and D. Hooper, Rev. Mod. Phys. **90**, 045002 (2018).

[13] R. L. Workman *et al.* (Particle Data Group), Prog. Theor. Exp. Phys. **2022**, 083C01 (2022).

[14] B. P. Abbott, R. Abbott, T. D. Abbott, M. R. Abernathy, F. Acernese, K. Ackley *et al.* (The LIGO Scientific and the Virgo Collaborations), Phys. Rev. Lett. **116**, 221101 (2016).

[15] B. P. Abbott, R. Abbott, T. D. Abbott, F. Acernese, K. Ackley *et al.* (The LIGO Scientific and the Virgo Collaborations), Phys. Rev. Lett. **118**, 221101 (2017).

[16] B. P. Abbott, R. Abbott, T. D. Abbott, F. Acernese, K. Ackley *et al.* (The LIGO Scientific and the Virgo Collaborations), Phys. Rev. Lett. **119**, 141101 (2017).

[17] B. P. Abbott, R. Abbott, T. D. Abbott, F. Acernese, K. Ackley *et al.* (The LIGO Scientific and the Virgo Collaborations), Astrophys. J. Lett. **851**, L35 (2017).

[18] B. P. Abbott, R. Abbott, T. D. Abbott, F. Acernese, K. Ackley *et al.* (The LIGO Scientific and the Virgo Collaborations), Phys. Rev. Lett. **121**, 161101 (2018).

[19] B. P. Abbott, R. Abbott, T. D. Abbott, M. R. Abernathy, F. Acernese, K. Ackley *et al.* (The LIGO Scientific and the Virgo Collaborations), Astrophys. J. Lett. **818**, L22 (2016).

[20] B. P. Abbott, R. Abbott, T. D. Abbott, M. R. Abernathy, F. Acernese, K. Ackley *et al.* (The LIGO Scientific and the Virgo Collaborations), Phys. Rev. Lett. **116**, 241103 (2016).

[21] B. P. Abbott, R. Abbott, T. D. Abbott, M. R. Abernathy, F. Acernese, K. Ackley *et al.* (The LIGO Scientific and the Virgo Collaborations), Phys. Rev. Lett. **116**, 061102 (2016).

[22] B. P. Abbott, R. Abbott, T. D. Abbott, F. Acernese, K. Ackley *et al.* (The LIGO Scientific and the Virgo Collaborations), Phys. Rev. Lett. **119**, 161101 (2017).

[23] B. P. Abbott *et al.*, Astrophys. J. Lett. **848**, L12 (2017).

[24] P. Routaray, H. C. Das, S. Sen, B. Kumar, G. Panotopoulos, and T. Zhao, Phys. Rev. D **107**, 103039 (2023).

[25] B. Kain, Phys. Rev. D **103**, 043009 (2021).

[26] G. Panotopoulos and I. Lopes, Phys. Rev. D **96**, 083004 (2017).

[27] H. C. Das, A. Kumar, B. Kumar, and S. K. Patra, Galaxies **10**, 14 (2022).

[28] L. Lopes and D. Menezes, J. Cosmol. Astropart. Phys. 05 (2018) 038.

[29] S. Shakeri and D. R. Karkevandi, Phys. Rev. D **109**, 043029 (2024).

[30] O. Lourenço, T. Frederico, and M. Dutra, Phys. Rev. D **105**, 023008 (2022).

[31] H. C. Das, A. Kumar, B. Kumar, S. K. Biswal, T. Nakatsukasa, A. Li, and S. K. Patra, Mon. Not. R. Astron. Soc. **495**, 4893 (2020).

[32] H. C. Das, A. Kumar, and S. K. Patra, Mon. Not. R. Astron. Soc. **507**, 4053 (2021).

[33] O. Lourenço, C. H. Lenzi, T. Frederico, and M. Dutra, Phys. Rev. D **106**, 043010 (2022).

[34] A. Quddus, G. Panotopoulos, B. Kumar, S. Ahmad, and S. K. Patra, J. Phys. G **47**, 095202 (2020).

[35] H. C. Das, A. Kumar, and S. K. Patra, Phys. Rev. D **104**, 063028 (2021).

[36] M. Dutra, C. H. Lenzi, and O. Lourenço, Mon. Not. R. Astron. Soc. **517**, 4265 (2022).

[37] Y. Dengler, J. Schaffner-Bielich, and L. Tolos, Phys. Rev. D **105**, 043013 (2022).

[38] E. Giangrandi, V. Sagun, O. Ivanytskyi, C. Providência, and T. Dietrich, Astrophys. J. **953**, 115 (2023).

[39] D. Rafiei Karkevandi, S. Shakeri, V. Sagun, and O. Ivanytskyi, Phys. Rev. D **105**, 023001 (2022).

[40] H. C. Das, A. Kumar, S. K. Biswal, and S. K. Patra, Phys. Rev. D **104**, 123006 (2021).

[41] J. C. Jiménez and E. S. Fraga, Universe **8**, 34 (2022).

[42] C. H. Lenzi, M. Dutra, O. Lourenço, L. L. Lopes, and D. P. Menezes, Eur. Phys. J. C **83**, 266 (2023).

[43] G. Lalazissis, S. Karatzikos, R. Fossion, D. P. Arteaga, A. Afanasjev, and P. Ring, Phys. Lett. B **671**, 36 (2009).

[44] B.-A. Li, L.-W. Chen, and C. M. Ko, Phys. Rep. **464**, 113 (2008).

[45] M. Dutra, O. Lourenço, S. S. Avancini, B. V. Carlson, A. Delfino, D. P. Menezes, C. Providência, S. Typel, and J. R. Stone, Phys. Rev. C **90,** 055203 (2014).

[46] B. V. Carlson, M. Dutra, O. Lourenço, and J. Margueron, Phys. Rev. C **107,** 035805 (2023).

[47] A. Das, T. Malik, and A. C. Nayak, Phys. Rev. D **105,** 123034 (2022).

[48] A. Kumar, H. C. Das, and S. K. Patra, Mon. Not. R. Astron. Soc. **513,** 1820 (2022).

[49] J. M. Cline, P. Scott, K. Kainulainen, and C. Weniger, Phys. Rev. D **88,** 055025 (2013).

[50] J. M. Cline, K. Kainulainen, P. Scott, and C. Weniger, Phys. Rev. D **92,** 039906 (2015).

[51] A. Tan, M. Xiao, X. Cui, X. Chen, Y. Chen, D. Fang, C. Fu, K. Giboni, F. Giuliani, H. Gong, X. Guo, K. Han, S. Hu, X. Huang, X. Ji, Y. Ju et al. (PandaX-II Collaboration), Phys. Rev. Lett. **117,** 121303 (2016).

[52] D. S. Akerib, S. Alsum, H. M. Araújo, X. Bai, A. J. Bailey, J. Balajthy, P. Beltrame, E. P. Bernard, A. Bernstein, T. P. Biesiadzinski, E. M. Boulton, R. Bramante, P. Brás, D. Byram, S. B. Cahn, M. C. Carmona-Benitez, C. Chan, A. A. Chiller, C. Chiller et al. (LUX Collaboration), Phys. Rev. Lett. **118,** 021303 (2017).

[53] L. Marini, L. Pagani, P. Agnes, T. Alexander, A. Alton, K. Arisaka, H. O. Back, B. Baldin, K. Biery, G. Bonfini, M. Bossa, A. Brigatti, J. Brodsky, F. Budano, L. Cadonati, F. Calaprice, N. Canci, A. Candela, H. Cao et al., Nuovo Cimento C Geophys. Space Phys. C **39,** 247 (2016).

[54] G. Baym, C. Pethick, and P. Sutherland, Astrophys. J. **170,** 299 (1971).

[55] J. Xu, L.-W. Chen, B.-A. Li, and H.-R. Ma, Astrophys. J. **697,** 1549 (2009).

[56] C. Gonzalez-Boquera, M. Centelles, X. Viñas, and T. R. Routray, Phys. Rev. C **100,** 015806 (2019).

[57] J. Xu, L.-W. Chen, B.-A. Li, and H.-R. Ma, Phys. Rev. C **79,** 035802 (2009).

[58] L. Lindblom and S. L. Detweiler, Astrophys. J. Suppl. Ser. **53,** 73 (1983).

[59] S. Detweiler and L. Lindblom, Astrophys. J. **292,** 12 (1985).

[60] T. Damour and A. Nagar, Phys. Rev. D **80,** 084035 (2009).

[61] T. Binnington and E. Poisson, Phys. Rev. D **80,** 084018 (2009).

[62] E. E. Flanagan and T. Hinderer, Phys. Rev. D **77,** 021502 (2008).

[63] F. J. Fattoyev, J. Carvajal, W. G. Newton, and B.-A. Li, Phys. Rev. C **87,** 015806 (2013).

[64] T. Malik, N. Alam, M. Fortin, C. Providência, B. K. Agrawal, T. K. Jha, B. Kumar, and S. K. Patra, Phys. Rev. C **98,** 035804 (2018).

[65] N. Hornick, L. Tolos, A. Zacchi, J.-E. Christian, and J. Schaffner-Bielich, Phys. Rev. C **98,** 065804 (2018).

[66] B. Kumar, S. K. Biswal, and S. K. Patra, Phys. Rev. C **95,** 015801 (2017).

[67] T. Hinderer, B. D. Lackey, R. N. Lang, and J. S. Read, Phys. Rev. D **81,** 123016 (2010).

[68] J. D. V. Arbañil, C. V. Flores, C. H. Lenzi, and J. M. Z. Pretel, Phys. Rev. D **107,** 124016 (2023).

[69] C. Vásquez Flores, A. Parisi, C.-S. Chen, and G. Lugones, J. Cosmol. Astropart. Phys. 06 (2019) 051.

[70] T. E. Riley et al., Astrophys. J. Lett. **887,** L21 (2019).

[71] M. Miller et al., Astrophys. J. Lett. **887,** L24 (2019).

[72] T. E. Riley et al., Astrophys. J. Lett. **918,** L27 (2021).

[73] M. C. Miller et al., Astrophys. J. Lett. **918,** L28 (2021).

[74] H. Cromartie et al. (NANOGrav Collaboration), Nat. Astron. **4,** 72 (2019).

[75] J. Antoniadis et al., Science **340,** 6131 (2013).

[76] P. Demorest, T. Pennucci, S. Ransom, M. Roberts, and J. Hessels, Nature (London) **467,** 1081 (2010).